Wireless Networks (2023) 29:843–855
https://doi.org/10.1007/s11276-022-03178-4

ORIGINAL PAPER

Generalized BER of MCIK-OFDM with imperfect CSI: selection combining GD versus ML receivers

Vu-Duc Ngo[1] · Thien Van Luong[2] · Nguyen Cong Luong[2] · Minh-Tuan Le[3] · Thi Thanh Huyen Le[4] · Xuan-Nam Tran[4]

Accepted: 18 October 2022 / Published online: 1 November 2022

Abstract
This paper analyzes the bit error rate (BER) of multicarrier index keying—orthogonal frequency division multiplexing (MCIK-OFDM) with selection combining (SC) diversity reception. Particularly, we propose a generalized framework to derive the BER for both the low-complexity greedy detector (GD) and maximum likelihood (ML) detector. Based on this, closed-form expressions for the BERs of MCIK-OFDM with the SC using either the ML or the GD are derived in presence of the channel state information (CSI) imperfection. The asymptotic analysis is presented to gain helpful insights into effects of different CSI conditions on the BERs of these two detectors. More importantly, we theoretically provide opportunities for using the GD instead of the ML under each specific CSI uncertainty, which depend on the number of receiver antennas and the M-ary modulation size. Finally, extensive simulation results are provided in order to validate our theoretical expressions and analysis.

Keywords MCIK-OFDM · Selection combining · OFDM-IM · Greedy detection (GD) · Maximum likelihood (ML) · Uncertain CSI

1 Introduction

Multicarrier index keying—orthogonal frequency division multiplexing (MCIK-OFDM) or the so-called OFDM with index modulation (OFDM-IM) is an emerging multicarrier scheme [1–3], which can offer higher energy efficiency and reliability over conventional OFDM. In MCIK-OFDM, a subset of subcarriers are active to carry data bits through both the conventional M-ary symbols and the indices of active subcarriers. Hence, MCIK-OFDM provides a promising trade-off between spectral efficiency (SE) and reliability compared to OFDM just by varying the number of active sub-carriers.

Recently, various MCIK or IM concepts have been proposed for OFDM, which can be found in the overview [4]. Particularly, the IM concept was first applied to OFDM-based multicarrier modulation in [1], and its enhanced version was proposed in [2], while its generalized version which independently applies the IM to different subcarrier groups was developed in [3]. For the performance analysis, in [5], a tight bound on the bit error rate (BER) of OFDM-IM using the maximum likelihood (ML)

✉ Thien Van Luong
thien.luongvan@phenikaa-uni.edu.vn

Vu-Duc Ngo
duc.ngovu@hust.edu.vn

Nguyen Cong Luong
luong.nguyencong@phenikaa-uni.edu.vn

Minh-Tuan Le
tuan.minh@mobifone.vn

Thi Thanh Huyen Le
huyen.ltt@mta.edu.vn

Xuan-Nam Tran
namtx@mta.edu.vn

[1] School of Electronics and Electrical Engineering, Hanoi University of Science and Technology, Hanoi 11657, Vietnam

[2] Faculty of Computer Science, Phenikaa University, Hanoi 12116, Vietnam

[3] MobiFone R &D Center, MobiFone Corporation, Hanoi 11312, Vietnam

[4] Advanced Wireless Communications Group, Le Quy Don Technical University, Ha Noi 11355, Vietnam

detection was derived. The MCIK concept was applied to multiple input multiple output (MIMO) systems in [6]. In [7], the generalized MCIK scheme with a variable number of active subcarriers was proposed. In [8], coordinate interleaving OFDM-IM was proposed to improve the diversity order. Also inspired by the MCIK concept, code index modulation (CIM) as well as its generalized version were studied in [9, 10]. Aiming to enhance the error performance of MCIK-OFDM, several transmit diversity schemes are reported in [11–14], in which the repetition code for either the index or M-ary symbol was used in [11–13], while the spreading code was used in [14]. Meanwhile, there are a number of studies in [15–17] that focus on improving the SE of MCIK-OFDM, where the IM-based transmitters are designed to increase the number of either index or M-ary bits. Recently, deep neural networks (DNNs) have been applied to the MCIK signal detection in [18, 19], which can provide a near-optimal performance at low runtime complexity. Additionally, the use of a DNN structure called autoencoder for jointly optimizing both the transmitter and receiver of multicarrier systems was reported in [20–23], where the resulting learning-based systems can even achieve better error performance than IM-based multicarrier systems. Finally, the IM technique was applied to visible light communications for improving the BER performance in [24].

Most of the aforementioned papers consider the ML or log-likelihood ratio (LLR) detector for MCIK-OFDM, which still has a significantly higher complexity than the classical OFDM. In [28], a low-complexity greedy detector (GD) was developed, which utilizes the energy detection method to estimate the active indices before decoding the M-ary symbols conveyed on these active sub-carriers. The outage probabilities and the pair-wise error probability of the GD under generalized fading were analyzed in [29] and [30], respectively. The symbol error probability (SEP) and BER of the GD in the presence of channel state information (CSI) imperfection were investigated in [25, 26], which reveal that the GD detector is less sensitive to imperfect CSI than its ML counterpart. In order to further improve the diversity gain of GD, MCIK-OFDM with hybrid GD and diversity receptions, namely selection combining (SC) and maximal ratio combining (MRC), was proposed in [27] to examine the SEP, however only for the perfect CSI case. Moreover, [27] fails to provide an analytical comparison between the MRC/SC-based GD and ML detectors, and its theoretical results are not tight, even at high signal-to-noise ratios (SNRs). Hence, this work is unable to provide a theoretical guideline of selecting a suitable detection method, particularly under different CSI uncertainties. Meanwhile, the GD shown in [25, 26] is more effective in practical systems with imperfect CSI. Therefore, it is worth investigating the performance of MCIK-OFDM with such low-complexity MRC/SC-based GD receivers under practical CSI uncertainty, and compare with its ML counterpart. In addition, the performance analysis of MCIK-OFDM using both MRC/SC and ML detection has been overlooked in the literature.

To address the aforementioned issues, in this paper, we first analyze and compare the BERs of MCIK-OFDM with the SC-based multiple-antenna receivers called MCIK-OFDM-SC, employing both ML and GD detectors, over uncertain CSI. In particular, the main contributions of this work compared with the existing works are listed in Table 1, and are summarized as follows:

- We propose a generalized framework for deriving the BERs of both the GD and the ML receivers for MCIK-OFDM, where the BER is represented as a linear combination of the SEP and index error probability (IEP) of the classical M-ary data symbols.
- Utilizing this proposed framework, tight, closed-form expressions for the BERs of MCIK-OFDM-SC employing both the GD and ML detectors are derived in presence of various CSI conditions, namely perfect CSI, and fixed or variable CSI uncertainties.
- Based on the derived expressions, asymptotic results are demonstrated to further investigate effects of different CSI uncertainties on the BERs of the two detectors. More importantly, we asymptotically develop conditions under which using the GD instead of the ML is desired for MCIK-OFDM-SC under each CSI condition, particularly when the number of antennas at the receiver increases.
- Simulation results are provided to validate the derived expressions, as well as theoretical guidelines for selecting detection type for each CSI condition. Unlike [27], our theoretical results are tight in a wide range of SNRs.

The rest of our paper is as follows. Section 2 describes MCIK-OFDM-SC and its signal detection under uncertain CSI. In Sect. 3 analyzes the BERs of both ML and GD, followed by asymptotic analysis in Sect. 4. Simulation results are performed in Sect. 5. Section 6 concludes our paper.

Notation: Lower-case bold and Upper-case bold letters and are used for vectors and matrices, respectively. $C(,)$ and $(.)^T$ denotes the binomial coefficient and transpose operation, respectively. The floor function is represented by $\lfloor . \rfloor$. $\mathcal{CN}(0, \sigma^2)$ stands for the complex Gaussian distribution with zero mean and variance σ^2. $\mathbb{E}\{.\}$ and $\mathcal{M}(.)$ present the expectation operator and the moment generating function (MGF), respectively.

Table 1 Contribution Comparison of MCIK-OFDM Performance Analysis

Contribution	[3]	[5]	[25]	[26]	[27]	This work
BER analysis	✓	✓		✓		✓
SEP analysis			✓		✓	
Imperfect CSI	✓		✓	✓		✓
SC-based multiple-antenna receivers					✓	✓
Greedy detector			✓	✓	✓	✓
ML detector	✓	✓	✓			✓
Asysmptotic analysis			✓	✓	✓	✓
Theoretical guideline for detector selection						✓

2 System model

2.1 MCIK-OFDM-SC

Consider a uplink single-input multi-output (SIMO) MCIK-OFDM scheme with $N_c = NG$ sub-carriers that are divided into G clusters with N sub-carriers per cluster. The transmitter employs a single antennas while the receiver uses L antennas. At the receiver, the SC technique is employed to combine signals received from L branches. Then, the output of the SC is used to estimate transmitted data bits using either the ML or the GD [27]. The resulting scheme is called as MCIK-OFDM-SC. Since each cluster independently operates the MCIK-OFDM technique, for simplicity and without loss of generality, hereinafter we address the problem of only one cluster, whose block diagram is illustrated in Fig. 1. Here, the role of OFDM framework is to make sub-carriers orthogonal to each other so that we can independently apply the MCIK concept to each cluster, reducing the transceiver complexity.

In every MCIK-OFDM transmission per cluster, only K out of N sub-carriers are activated to carry information bits with K complex M-ary symbols, while additional data bits are delivered by the indices of active sub-carriers. More specifically, p incoming bits are partitioned into two streams ($p = p_1 + p_2$) at the transmitter. Utilizing combinatorial method or look-up table (LUT) [3], the first p_1 bits are mapped to a pattern of K active sub-carriers. Denote by $\theta = \{\alpha_1, \ldots, \alpha_K\}$ the set of K active sub-carrier indices, where $\alpha_k \in \{1, \ldots, N\}$ for $k = 1, \ldots, K$. Note that θ can be referred to as an index symbol, which is identified by p_1 index bits. The remaining p_2 bits are mapped to K M-ary symbols. For given N, K and M, the number of index bits and symbol bits are given by $p_1 = \lfloor \log_2 C(N, K) \rfloor$ and $p_2 = K \log_2 M$, respectively. Denote by $\mathcal{S}$ the M-ary constellation. Using θ and K non-zero symbols (determined by p incoming bits), the transmitted signal for each cluster is given as $\mathbf{x} = [x(1), \ldots, x(N)]^T$, where $x(\alpha) = 0$ for $\alpha \notin \theta$ and $x(\alpha) \in \mathcal{S}$ for $\alpha \in \theta$. Here, note that the K non-zero data symbols conveyed on active sub-carriers are denoted as vector $\mathbf{s}$ in Fig. 1. The frequency domain signal $\mathbf{x}$ is then processed by the inverse fast Fourier transform (IFFT) before being transmitted to the receiver.

The received signal at the l-th antenna in the frequency domain, i.e., the signal obtained after the FFT, is given by

$$\mathbf{y}_l = \mathbf{H}_l \mathbf{x} + \mathbf{n}_l, \tag{1}$$

where $\mathbf{H}_l = \text{diag}\{h_l(1), \ldots, h_l(N)\}$ is the channel matrix between the transmitter and the l-th receiver antenna, while $\mathbf{n}_l = [n_l(1), \ldots, n_l(N)]^T$ is the noise vector with $n_l(\alpha) \sim \mathcal{CN}(0, N_0)$, for $\alpha = 1, \ldots, N$ and $l = 1, \ldots, L$. Particularly, $h_l(\alpha)$ represents the Rayleigh fading channel, which is identical and independent to each other, where $h_l(\alpha) \sim \mathcal{CN}(0, 1)$. Here, we assume that the cyclic prefix inserted to each OFDM symbol in the time domain is large enough to completely combat the inter-symbol interference [3]. As such, the average SNR per active sub-carrier is given by $\bar{\gamma} = \varphi E_s / N_0$, where E_s denotes the average power per non-zero M-ary symbol and $\varphi = N/K$ is the power allocation ratio.

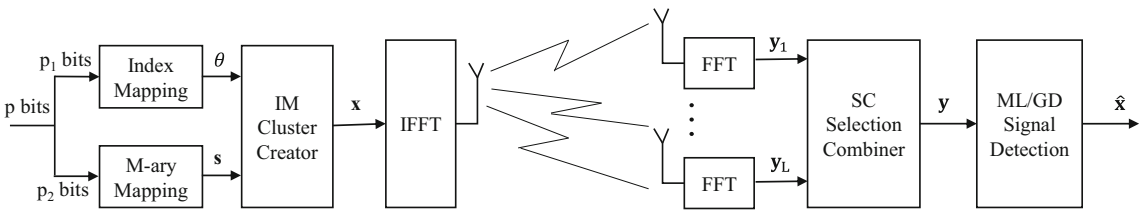

Fig. 1 The block diagram of MCIK-OFDM-SC

2.2 Post-combining detection under CSI uncertainty

We consider a practical MCIK-OFDM-SC system where the receiver imperfectly knows the CSI. Particularly, denote by $\hat{h_l}(\alpha)$ the estimate of the true channel $h_l(\alpha)$, and we have

$$\hat{h_l}(\alpha) = h_l(\alpha) - e_l(\alpha), \tag{2}$$

where $e_l(\alpha)$ represents the channel estimation error as being independent of $\hat{h_l}(\alpha)$ and $e_l(\alpha) \sim \mathcal{CN}(0, \epsilon^2)$, and $\hat{h_l}(\alpha) \sim \mathcal{CN}(0, 1-\epsilon^2)$, where $\epsilon^2 \in [0, 1)$ denotes the error variance.

For sub-carrier α, the l^*-th branch is selected as the output of the SC such that $l^* = \arg\max_l \left|\hat{h_l}(\alpha)\right|^2$. Hence, the output signal of the SC can be given by

$$\mathbf{y} = \mathbf{H}\mathbf{x} + \mathbf{n}, \tag{3}$$

where $\mathbf{H} = \text{diag}\{h(1), \ldots, h(N)\}$ denotes the channel matrix of the SC and the corresponding noise vector is $\mathbf{n} = [n(1), \ldots, n(N)]^T$, where $h(\alpha) = h_{l^*}(\alpha)$ and $n(\alpha) = n_{l^*}(\alpha)$ for $\alpha = 1, \ldots, N$. Notice in (3) that $\mathbf{y} = [y(1), \ldots, y(N)]^T$, with $y(\alpha) = h(\alpha)x(\alpha) + n(\alpha)$.

Let $\hat{h}(\alpha)$ be the estimate of $h(\alpha)$, i.e., $\hat{h}(\alpha) = \hat{h_{l^*}}(\alpha)$. Based on $\mathbf{y}$ and $\hat{h}(\alpha)$, either the ML or the GD can be employed for the signal detection as follows.

2.2.1 Post-combining ML

Under imperfect CSI, the estimated signal $\hat{\mathbf{x}}$ is calculated by the ML criterion as

$$\hat{\mathbf{x}} = \arg\min_{\mathbf{x}} \left\|\mathbf{y} - \hat{\mathbf{H}}\mathbf{x}\right\|^2,$$

where $\hat{\mathbf{H}} = \text{diag}\left\{\hat{h}(1), \ldots, \hat{h}(N)\right\}$ denotes the estimate of the channel matrix after the SC. Utilizing $\hat{\mathbf{x}}$, the index symbol $\hat{\theta}$ and K non-zero symbols $x(\alpha)$ with $\alpha \in \hat{\theta}$ are recovered.

2.2.2 Post-combining GD

Post-combining GD makes best antenna selections per sub-carrier before GD processing. For given $\mathbf{H}$, the GD detects signals through two following steps. Firstly, the active indices are estimated by K sub-carriers that have the largest SC-output energies, i.e., $|y(\alpha)|^2$. Secondly, the non-zero M-ary symbols are detected by applying the ML decision to activated sub-carrier α as

$$x(\alpha) = \arg\min_{x(\alpha)\in\mathcal{S}} \left|y(\alpha) - \hat{h}(\alpha) \times (\alpha)\right|^2. \tag{4}$$

Note that the GD detector has not only lower complexity, but also less sensitivity to CSI imperfection, than the ML detector [26]. However, when the number of antennas is limited to one, the ML still perform much better than GD under certain CSI conditions, especially when M is small (e.g., $M = 2, 4$) [25].

As a result, we are prompted to examine the BER performance of both the GD and the ML in MCIK-OFDM-SC, in order to understand if the post-combining GD receiver benefits from diversity gain. For this, we intend to derive the closed-form expressions for the BERs of the two detectors, taking CSI uncertainty into consideration in the next section.

3 BER analysis with CSI uncertainty

We note that the ML performs the same performance as the log-likelihood ratio (LLR) detector [12] which also has two separate steps as the GD. Thus, we now introduce a generalized framework to derive the BERs of both the ML and the GD. Particularly, we consider bit error event consisting of two parts: the index bit error (p_1 bits) and the symbol bit error (p_2 bits). Let P_1 be the index BER (IBER) and P_2 be the symbol BER (SBER). Then, the BER of either the ML or the GD is given by

$$P_b = \frac{p_1 P_1 + p_2 P_2}{p_1 + p_2}. \tag{5}$$

The IBER and the SBER are obtained by [26]

$$P_1 \approx \eta \overline{P}_I / 2, \tag{6}$$

$$P_2 \leq \frac{\overline{P}_I}{2K} + \frac{\overline{P}_M}{\log_2 M}, \tag{7}$$

where $\overline{P}_I$ denotes the average index error probability (IEP), $\eta = 1$ for $N > 2$ and $\eta = 2$ for $N = 2$, and $\overline{P}_M$ is the average SEP of the M-ary symbol detection as long as the activated indices are correctly detected. Plugging (6) and (7) into (5), the generalized BER expression for both the ML and the GD is given by

$$P_b \approx \frac{(\eta p_1 + m)\overline{P}_I/2 + K\overline{P}_M}{p}, \tag{8}$$

where $m = \log_2 M$ and $p = p_1 + p_2$.

Remark 1 As seen from (8), when K increases to N, the BER of either the ML or the GD approaches that of classical OFDM, which is $\overline{P}_M/m$. As a result, the performance gap between these two detectors gets smaller when K gets larger.

Remark 2 $\overline{P}_M$ in (8) is the same for both the ML and the GD, while $\overline{P}_I$ depends on the detection type employed. Thus, to find out the BER expressions for the GD and the ML in MCIK-OFDM-SC, we need to derive $\overline{P}_I$ for them, considering CSI uncertainty. Meanwhile, $\overline{P}_M$ is provided in the following lemma when the M-ary PSK modulation is employed.

Lemma 1 *Under CSI uncertainty with the error variance ϵ^2, the average SEP of the conventional M-ary PSK symbol detection in MCIK-OFDM-SC is approximated by*

$$\overline{P}_M \approx \frac{\xi}{12}\left\{\frac{L!}{\prod_{l=1}^{L}\left[l+\frac{(1-\epsilon^2)\rho\bar{\gamma}}{1+\epsilon^2\bar{\gamma}}\right]}+\frac{3L!}{\prod_{l=1}^{L}\left[l+\frac{4(1-\epsilon^2)\rho\bar{\gamma}}{3(1+\epsilon^2\bar{\gamma})}\right]}\right\}, \tag{9}$$

where $\rho=\sin^2(\pi/M)$, $\xi=1$ for $M=2$ and $\xi=2$ for $M>2$.

Proof See Appendix A. □

3.1 BER for ML with SC reception and CSI uncertainty

We first consider the IEP of the ML in MCIK-OFDM with the SC and imperfect CSI. Denote by P_{I_1} the instantaneous IEP of the ML, which is approximated by [25]

$$P_{I_1} \approx \frac{K}{N}\sum_{\alpha=1}^{N}\sum_{\tilde{\alpha}\neq\alpha=1}^{N-K}\left[\frac{1}{12}e^{-\frac{\bar{\gamma}\left(\hat{v}_\alpha+\hat{v}_{\tilde{\alpha}}\right)}{4+2\bar{\gamma}\epsilon^2}}+\frac{1}{4}e^{-\frac{2\bar{\gamma}\left(\hat{v}_\alpha+\hat{v}_{\tilde{\alpha}}\right)}{6+3\bar{\gamma}\epsilon^2}}\right], \tag{10}$$

where $\hat{v}_\alpha=\left|\hat{h}(\alpha)\right|^2$, $\hat{v}_{\tilde{\alpha}}=\left|\hat{h}(\tilde{\alpha})\right|^2$.

Denote $\hat{v}_\Sigma=\hat{v}_\alpha+\hat{v}_{\tilde{\alpha}}$. The moment generating function (MGF) of $\hat{v}_\Sigma$ can be attained by $\mathcal{M}_{\hat{v}_\Sigma}(s)=\mathcal{M}^2_{\hat{v}}(s)$, where $\mathcal{M}_{\hat{v}}(s)$ is the MGF of $\hat{v}_\alpha$ which is given in (33). Here, applying the MGF approach to (10), we obtain the average IEP of the ML with the SC and uncertain CSI as follows

$$\overline{P}_{I_1} \approx \frac{\Psi_1}{12}\left\{\frac{(L!)^2}{\prod_{l=1}^{L}\left[l+\frac{(1-\epsilon^2)\bar{\gamma}}{4+2\bar{\gamma}\epsilon^2}\right]^2}+\frac{3(L!)^2}{\prod_{l=1}^{L}\left[l+\frac{2(1-\epsilon^2)\bar{\gamma}}{6+3\bar{\gamma}\epsilon^2}\right]^2}\right\}, \tag{11}$$

where $\Psi_1=K(N-K)$.

As observed from (11), note that as $L=1$, the average IEP of the ML in (11) reduces to [25, Eq. (16)]. In addition, $\overline{P}_{I_1}$ mainly relies on N, K and L, while being less influenced by the modulation size M.

Finally, the BER of the ML (denoted by P_{b_1}) can be obtained by inserting (9) and (11)–(8) as

$$P_{b_1} \approx \frac{\widetilde{\Psi}_1}{24p}\left\{\frac{(L!)^2}{\prod_{l=1}^{L}\left[l+\frac{(1-\epsilon^2)\bar{\gamma}}{4+2\bar{\gamma}\epsilon^2}\right]^2}+\frac{3(L!)^2}{\prod_{l=1}^{L}\left[l+\frac{2(1-\epsilon^2)\bar{\gamma}}{6+3\bar{\gamma}\epsilon^2}\right]^2}\right\} + \frac{K\xi}{12p}\left\{\frac{L!}{\prod_{l=1}^{L}\left[l+\frac{(1-\epsilon^2)\rho\bar{\gamma}}{1+\epsilon^2\bar{\gamma}}\right]}+\frac{3L!}{\prod_{l=1}^{L}\left[l+\frac{4(1-\epsilon^2)\rho\bar{\gamma}}{3(1+\epsilon^2\bar{\gamma})}\right]}\right\}, \tag{12}$$

where $\widetilde{\Psi}_1=\Psi_1(\eta p_1+m)=K(N-K)(\eta p_1+m)$.

It is shown from (12) that increasing L improves the BER of the ML. Moreover, for given N, L and $\bar{\gamma}$, the BER P_{b_1} depends on both K and ϵ^2. For example, when K gets larger, the second term, which is related to the M-ary symbol detection, will dominate over P_{b_1}. Especially, as $K=N$, (12) reduces to the BER of the classical OFDM.

3.2 BER for GD with SC reception and CSI uncertainty

In MCIK-OFDM with the single antenna used at both the transmitter and the receiver, the IEP of the GD is independent of CSI conditions [26]. However, this is no longer true when employing the SC for MCIK-OFDM. Particularly, the instantaneous IEP of the GD is given by [26, 27]

$$P_{I_2}=\frac{K}{N}\sum_{\alpha=1}^{N}\sum_{i=1}^{N-K}\frac{(-1)^{i+1}C(N-K,i)}{i+1}e^{-\frac{i\bar{\gamma}v_\alpha}{i+1}}, \tag{13}$$

where $v_\alpha=|h(\alpha)|^2$ which is obviously affected by the estimate $\hat{h}_l(\alpha)$ due to $h(\alpha)=h_{l^*}(\alpha)$ with $l^*=\max_l\left|\hat{h}_l(\alpha)\right|^2$. The detailed derivation of (13) over Rayleigh fading channels was presented in [28], which is not included here for the sake of brevity. Thus, the IEP of the GD in our system depends on the channel estimation errors. This makes the derivation of the average IEP for this detector non-trivial as follows.

First, it is needed to figure out the MGF of v_α. Using (2), $h(\alpha)$ can be represented as $h(\alpha)=e^{j\phi}\left|\hat{h}(\alpha)\right|+e(\alpha)=e^{j\phi}\left(\left|\hat{h}(\alpha)\right|+\tilde{e}(\alpha)\right)$, where $\tilde{e}(\alpha)=e^{-j\phi}e(\alpha)\sim\mathcal{CN}(0,\epsilon^2)$ and ϕ denotes the argument of $\hat{h}(\alpha)$. This results in

$$|h(\alpha)|^2=\left|\left|\hat{h}(\alpha)\right|+\tilde{e}(\alpha)\right|^2. \tag{14}$$

From (14), the MGF of v_α can be computed as

$$\begin{aligned}\mathcal{M}_v(t)&=\mathbb{E}_{|h(\alpha)|^2}\left\{e^{|h(\alpha)|^2t}\right\}\\&=\mathbb{E}_{\left|\hat{h}(\alpha)\right|^2}\left\{\mathbb{E}_{\left|\left|\hat{h}(\alpha)\right|+\tilde{e}(\alpha)\right|^2}\left\{e^{\left|\left|\hat{h}(\alpha)\right|+\tilde{e}(\alpha)\right|^2t}\right\}\right\}\\&=\int_0^\infty f_{\left|\hat{h}(\alpha)\right|^2}(x)\mathcal{M}_{\left|\left|\hat{h}(\alpha)\right|+\tilde{e}(\alpha)\right|^2}(t)dx,\end{aligned} \tag{15}$$

which motivates us to propose the following lemma.

Lemma 2 *Let* $\tilde{e}(\alpha) \sim \mathcal{CN}(0, \epsilon^2)$, *then for given* $\left|\hat{h}(\alpha)\right|^2$, *the MGF of* $\left|\left|\hat{h}(\alpha)\right| + \tilde{e}(\alpha)\right|^2$ *is given by*

$$\mathcal{M}_{\left|\left|\hat{h}(\alpha)\right|+\tilde{e}(\alpha)\right|^2}(t) = \frac{e^{\frac{\left|\hat{h}(\alpha)\right|^2 t}{1-\epsilon^2 t}}}{1-\epsilon^2 t}. \tag{16}$$

Proof See Appendix B. □

Inserting (32) and (16) into (15), through simple manipulations, we obtain

$$\mathcal{M}_v(t) = \frac{L!}{(1-\epsilon^2 t)\prod_{l=1}^{L}\left[l - \frac{(1-\epsilon^2)t}{1-\epsilon^2 t}\right]}. \tag{17}$$

Note that to the best of our knowledge, the approach to derive the MGF of v_α in closed-form (17) is novel. This interestingly results in a simple, exact closed-form expression for the average IEP of the GD with the SC and uncertain CSI, by applying the MGF approach to (13) and using (17), as

$$\overline{P}_{I_1} = K\sum_{i=1}^{N-K}\frac{(-1)^{i+1}C(N-K,i)L!}{(i+1+i\epsilon^2\bar{\gamma})\prod_{l=1}^{L}\left[l + \frac{(1-\epsilon^2)i\bar{\gamma}}{i+1+i\epsilon^2\bar{\gamma}}\right]}. \tag{18}$$

As observed from (18), when $L = 1$, the expression for $\overline{P}_I$ becomes [26, Eq. (8)] which no longer depends on ϵ^2. In addition, as $L > 1$, the IEP performance suffers from a degradation caused by CSI uncertainty, i.e., ϵ^2. Note that for any $\epsilon^2 \in [0, 1)$, $\overline{P}_{I_1}$ always tends to 0 as $\bar{\gamma}$ increases to infinity, even for the worst case of $\epsilon^2 = 1$.

Finally, the BER of the GD with the SC and uncertain CSI can be attained by substituting (9) and (18)–(8) as follows:

$$P_{b_2} \approx \frac{K(\eta p_1 + m)}{2p}\sum_{i=1}^{N-K}\frac{(-1)^{i+1}C(N-K,i)L!}{(i+1+i\epsilon^2\bar{\gamma})\prod_{l=1}^{L}\left[l + \frac{(1-\epsilon^2)i\bar{\gamma}}{i+1+i\epsilon^2\bar{\gamma}}\right]} + \frac{K\xi}{12p}\left\{\frac{L!}{\prod_{l=1}^{L}\left[l + \frac{(1-\epsilon^2)\rho\bar{\gamma}}{1+\epsilon^2\bar{\gamma}}\right]} + \frac{3L!}{\prod_{l=1}^{L}\left[l + \frac{4(1-\epsilon^2)\rho\bar{\gamma}}{3(1+\epsilon^2\bar{\gamma})}\right]}\right\}. \tag{19}$$

Observe from (19) that different from MCIK-OFDM with the single antenna [26], where ϵ^2 affects only the term related to the M-ary symbol detection, in MCIK-OFDM-SC having multiple anttenas, ϵ^2 influences on both the index detection error and the M-ary symbol detection error. As $L = 1$, (19) reduces to [26, Eq. (15)], which confirms the accuracy of our derivation for the BER expression of MCIK-OFDM-SC.

4 Asymptotic analysis

We now carry out the asymptotic analysis for the BERs of both ML and GD detectors at high SNRs and in a large number of antennas. In particular, we investigate the impact of various CSI uncertainties, namely perfect CSI, fixed CSI uncertainty, and minimum mean square (MMSE) based variable CSI uncertainty. In addition, the performance comparison between the two detectors is provided. This allows to recommend that when the GD should be used under each CSI condition as the number of antennas increases.

Note that existing studies [25–27] have not provided any analytical comparisons between the ML and the GD such as the behavior of the coding gain gap between them when the number of antennas changes. Moreover, [27] even has not included any asymptotic analysis for the GD with the SC.

4.1 Perfect CSI ($\epsilon^2 = 0$)

As $\epsilon^2 = 0$ and $\bar{\gamma}$ tends to infinity, the BERs in (12) and (19) can be asymptotically approximated by

$$P_{b_1} \approx \Upsilon\left(\frac{\xi\Omega}{6\rho^L}\right)\frac{1}{\gamma_0^L}, \tag{20}$$

$$P_{b_2} \approx \Upsilon\left[(\eta p_1 + m)\omega + \frac{\xi\Omega}{6\rho^L}\right]\frac{1}{\gamma_0^L}, \tag{21}$$

where $\Upsilon = K^{L+1}L!/2pN^L$, $\Omega = 1 + 3^{L+1}/4^L$, $\omega = \sum_{i=1}^{N-K}(-1)^{i+1}C(N-K,i)(1+i)^{L-1}/i^L$, and $\gamma_0 = E_s/N_0$ is the average SNR per sub-carrier.

As observed from (20) and (21), both the ML and the GD attain a diversity order of L under perfect CSI. Moreover, for given N and L, a smaller K provides lower BERs.

Regarding the comparison between the GD and the ML, we consider the coding gain attained by the ML over the GD under perfect CSI (denoted by Δ_1), which can be denoted by $\Delta_1 = 10\log_{10}(P_{b_2}/P_{b_1})^{1/L}$. Using (20) and (21), we have

$$\Delta_1 = \frac{10}{L}\log_{10}(1+\eta_1)\,(\text{dB}), \tag{22}$$

where $\eta_1 = 6(\eta p_1 + m)\omega\rho^L/\xi\Omega$. Based on this result, we introduce the following theorem.

Theorem 1 *Consider MCIK-OFDM with the SC and perfect CSI. For* $M = 2$, *the ML performs better than the GD in terms of the BER by* 3 *dB, at large L, i.e,* $\lim_{L\to\infty}\Delta_1 \approx 3$ *(dB). For* $M \geq 4$, *the BER of GD approaches to that of ML when increasing L, i.e.,* $\lim_{L\to\infty}\Delta_1 = 0$ *(dB). Especially, when* $M \geq 8$, *the BERs of the two*

detectors rapidly converge to each other as L increases, i.e., $\lim_{L\to\infty}\eta_1 = 0$.

Proof Since ω in (21) can be approximated by $\omega \approx (N-K)2^{L-1}$ at large L, we approximate η_1 at large L as

$$\eta_1 \approx \beta_1 \lambda_1^L, \tag{23}$$

where $\lambda_1 = 2\rho$, recalling $\rho = \sin^2(\pi/M)$, and $\beta_1 = 3(\eta p_1 + m)(N-K)/\xi\Omega$ which decreases when increasing L due to $\Omega = 1 + 3^{L+1}/4^L$.

For $M = 2$, we obtain $\lambda_1 = 2$, thus $\eta_1 \approx \beta_1 2^L$. Using (22), $\lim_{L\to\infty}\Delta_1 = \lim_{L\to\infty}(10/L)\log_{10}(1+\beta_1 2^L) = 10\log_{10}2 \approx 3$ (dB).

For $M \geq 4$, we obtain $\lambda_1 \leq 1$, thus $1 < \eta_1 \leq 1+\beta_1$. This leads to $\lim_{L\to\infty}\Delta_1 = 0$ (dB).

For $M \geq 8$, we attain $\lambda_1 \leq 2\sin^2(\pi/8) < 0.3$, which results in $\lim_{L\to\infty}\eta_1 = \lim_{L\to\infty}\beta_1\lambda_1^L = 0$. □

Remark 3 From Theorem 1, it is recommended that the GD should be used rather than the ML under perfect CSI as $M \geq 8$, especially when L gets larger. This is because the GD can achieve a nearly optimal BER at a significantly lower complexity than the ML detector for large M and L. Note that the complexities of the ML and GD in MCIK-OFDM with the SC are $\mathcal{C}_{ML-SC} = N + 2CM^K$ and $\mathcal{C}_{GD-SC} = 2N + 2KM$, respectively, where $C = 2^{p_1}$ [27]. Obviously, when K and M become larger, we attain $\mathcal{C}_{ML-SC} \gg \mathcal{C}_{GD-SC}$.

4.2 Fixed CSI uncertainty ($\epsilon^2 > 0$)

As $\epsilon^2 > 0$ is fixed, the BERs in (18) and (19) can be rewritten at high SNRs, respectively, as follows:

$$P_{b_1} \approx \underbrace{\frac{\widetilde{\Psi}_1}{24p}\left\{\frac{1}{\prod_{l=1}^{L}\left[1+\frac{(1-\epsilon^2)}{2l\epsilon^2}\right]^2} + \frac{3}{\prod_{l=1}^{L}\left[1+\frac{2(1-\epsilon^2)}{3l\epsilon^2}\right]^2}\right\}}_{A_1} + \frac{K\xi}{12p}\left\{\frac{1}{\prod_{l=1}^{L}\left[1+\frac{(1-\epsilon^2)\rho}{l\epsilon^2}\right]} + \frac{3}{\prod_{l=1}^{L}\left[1+\frac{4(1-\epsilon^2)\rho}{3l\epsilon^2}\right]}\right\}, \tag{24}$$

$$P_{b_2} \approx \frac{K\xi}{12p}\left\{\frac{1}{\prod_{l=1}^{L}\left[1+\frac{(1-\epsilon^2)\rho}{l\epsilon^2}\right]} + \frac{3}{\prod_{l=1}^{L}\left[1+\frac{4(1-\epsilon^2)\rho}{3l\epsilon^2}\right]}\right\}, \tag{25}$$

where we recall that $\widetilde{\Psi}_1 = K(N-K)(\eta p_1 + m)$.

As seen from (24) and (25), for fixed ϵ^2, there exists error floors on the BERs of both the ML and the GD, or equivalently, increasing the SNR does not improve the BER. Thus, these two detectors in this case achieve a zero diversity gain for any L. Furthermore, when L gets larger or ϵ^2 gets smaller, the error floors in (24) and (25) become lower.

The following theorem compares the BER between the ML and the GD in MCIK-OFDM with the SC and fixed ϵ^2.

Theorem 2 *In MCIK-OFDM using the SC under fixed CSI uncertainty, the GD achieves a better BER than the ML detector at high SNRs, i.e.,* $P_{b_1} > P_{b_2}$.

Proof It is shown from (24) and (25) that at high SNRs, $P_{b_1} = P_{b_2} + A_1 > P_{b_2}$, where the term A_1 is related to the index detection error of the ML. This concludes the proof.

Remark 4 As a result of Theorem 2, under fixed CSI imperfection, the GD is able to outperform the ML in terms of both the BER and computational complexity, even for any M. This is obviously contrary to the perfect CSI case, where the BER of ML is always lower than that of GD.

4.3 MMSE-based variable CSI uncertainty

Note that the error variance provided by the MMSE channel estimator is given by [26]

$$\epsilon^2 = \frac{1}{1+\gamma_0}, \tag{26}$$

which varies as a decreasing function of the SNR.

Inserting (26)–(12) and (19), we obtain the asymptotic BERs for the ML and the GD in this case as

$$P_{b_1} \approx \Upsilon\left[\frac{\xi\Omega(1+N/K)^L}{6\rho^L}\right]\frac{1}{\gamma_0^L}, \tag{27}$$

$$P_{b_2} \approx \Upsilon\left[\psi(\eta p_1 + m) + \frac{\xi\Omega(1+N/K)^L}{6\rho^L}\right]\frac{1}{\gamma_0^L}, \tag{28}$$

where Υ and Ω are defined in (21), and $\psi = \sum_{i=1}^{N-K}(-1)^{i+1}C(N-K,i)(i+1+iN/K)^{L-1}/i^L$

As seen from (27) and (28), both the GD and the ML of MCIK-OFDM with the SC achieves the same diversity order of L in this case. However, due to the impact of MMSE channel estimation errors, the BERs in (27) and (28) are obviously greater than that of the perfect CSI case. For example, we can see from (20) and (27) that under the MMSE CSI imperfection, the ML endures a coding gain loss of $10\log_{10}(1+N/K)$ (dB) compared with the perfect CSI case.

As for the comparison in the BER between the ML and the GD, denote by Δ_2 the coding gain attained by the ML over GD detector under MMSE variable CSI uncertainty, which can be obtained from (27) and (28) as

$$\Delta_2 = \frac{10}{L}\log_{10}(1+\eta_2)\,(\text{dB}), \tag{29}$$

where $\eta_2 = 6\psi(\eta p_1 + m)\rho^L/\xi\Omega(1+N/K)^L$. Similar to Theorem 1, utilizing (29) we propose the following theorem.

Theorem 3 *Consider MCIK-OFDM using the SC and the MMSE-based variable CSI imperfection. For $M \geq 4$, the BERs of the ML and the GD rapidly converge to each other as increasing L, i.e., $\lim_{L\to\infty}\eta_2 = 0$. When $M = 2$, the ML performs better than the GD in terms of the BER by a coding gain of $10\log_{10}[1+K/(N+K)](dB)$, at large L, i.e., $\lim_{L\to\infty}\Delta_2 = 10\log_{10}[1+K/(N+K)]$ (dB), moreover $\lim_{L\to\infty}\Delta_2 < \lim_{L\to\infty}\Delta_1$.*

Proof Akin to Theorem 1, at large L, ψ in (28) can be approximated as $\psi \approx (N-K)(2+N/K)^{L-1}$. Thus,

$$\eta_2 \approx \beta_2\lambda_2^L, \tag{30}$$

where $\beta_2 = 6(\eta p_1 + m)(N-K)/\xi\Omega(2+N/K)$ which is a decreasing function of L and $\lambda_2 = \rho[1+K/(N+K)]$.

For $M \geq 4$, we have $\lambda_2 \leq [1+K/(N+K)]/2 < 1$ for any $K < N$. Hence, $\lim_{L\to\infty}\eta_2 = \lim_{L\to\infty}\beta_2\lambda_2^L = 0$.

For $M = 2$, we attain $\lambda_2 = 1+K/(N+K) > 1$. Thus, $\lim_{L\to\infty}\Delta_2 = (10/L)\log_{10}[1+K/(N+K)]^L = 10\log_{10}[1+K/(N+K)]$ (dB). Moreover, due to $1+K/(N+K) < 1.5$, $\lim_{L\to\infty}\Delta_2 < (10/L)\log_{10}(1.5^L) \approx 1.76 < \lim_{L\to\infty}\Delta_1 \approx 3$ (dB). □

Remark 5 Compared to the perfect CSI case (Theorem 1), Theorem 3 indicates that for given M, the performance gap between the two detectors under uncertain CSI gets smaller than that under perfect CSI. Therefore, the GD becomes more attractive than the ML under the MMSE CSI condition, particularly when the receiver has more antennas.

5 Simulation results

We provide simulation results for MCIK-OFDM-SC having $N_c = 128$ total sub-carriers, which are divided into G clusters, each having N sub-channels. For illustrations, we consider $N \in \{2,4\}$, $K < 4$, $M \in \{2,4,8\}$, and $L \in \{1,2,4,8,12\}$. The BER simulation results for the GD are compared to the ML under various MCIK parameters and CSI conditions.

5.1 Accuracy of theoretical and asymptotic expressions

Figure 2 depicts the simulation results of MCIK-OFDM-SC using the GD, along with the theoretical and asymptotic BER expressions when $(N,K,M,L) = (4,1,4,2)$, under various CSI conditions. As observed from Fig. 2, the theoretical BER expressions derived for the GD are very tight, i.e., very close to simulation results in a broad range of SNRs, while the asymptotic results are accurate in high SNR regions. This observation clearly confirms the accuracy of our theoretical analysis provided in Sects. 3 and 4. In addition, under fixed or variable ϵ^2, the GD suffers from a considerable loss in the BER compared to the perfect CSI case ($\epsilon^2 = 0$). For example, at BER of 10^{-3} in Fig. 2, the loss of SNR gain caused by fixed or variable CSI uncertainty is more than 4 dB. Note that a similar observation can be seen in Fig. 3 for the ML detector.

5.2 BER under perfect CSI

Figure 4 depicts the BERs for the ML and the GD in MCIK-OFDM-SC under perfect CSI, with $(N,K,M) = (2,1,2)$ and $L = 1,2,4,8$. As observed from Fig. 4, the ML always outperforms the GD even as L increases. For instance, as $L = 8$, at BER of 10^{-4}, the ML achieves the SNR gain of 3 dB over the GD. This confirms Theorem 1 as $M = 2$.

In Fig. 5, the BER comparison between the two detectors under perfect CSI is illustrated for MCIK-OFDM-SC with $(N,K,M) = (4,3,4)$ and $L = 1,2,8$. It is shown from Fig. 5 that when $M = 4$, the BER of the GD approaches to that of the ML as L gets larger. In particular, at BER of 10^{-3}, the coding gain attained by the ML over the GD is about 5 dB when $L = 1$, while this gain reduces to only 1 dB when $L = 8$. This validates Theorem 1 for the case of $M = 4$.

Figure 6 illustrates the BERs for the ML and the GD when $(N,K,M) = (4,2,8)$ and $L = 1,2,4,8$. It is clear

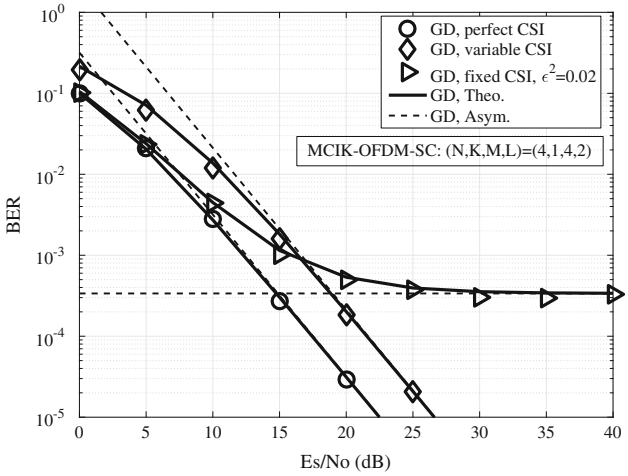

Fig. 2 BER of the GD detector in MCIK-OFDM-SC under various CSI conditions, with $(N,K,M,L) = (4,1,4,2)$

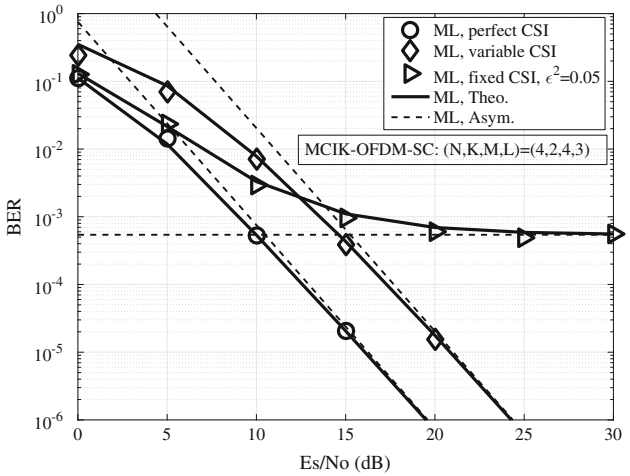

Fig. 3 BER of the ML detector in MCIK-OFDM-SC under various CSI conditions, with $(N, K, M, L) = (4, 2, 4, 3)$

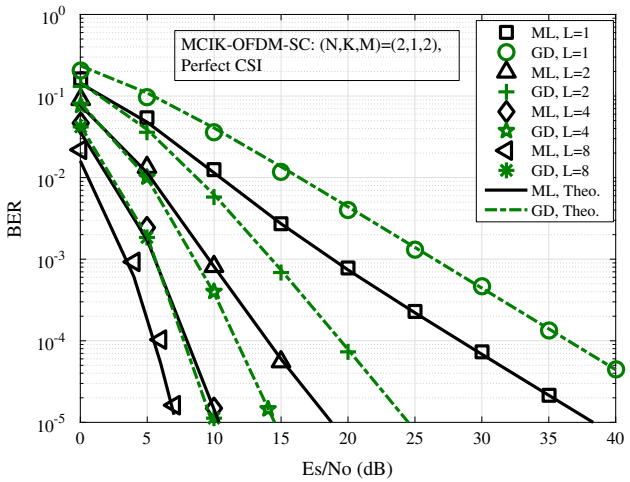

Fig. 4 BER comparison between the ML and the GD in MCIK-OFDM-SC under perfect CSI, with $(N, K, M) = (2, 1, 2)$ and $L = 1, 2, 4, 8$

from this figure that the BER of GD rapidly tends to that of the ML as L increases. Specifically, as $L = 4$, the performance gap between these two detectors becomes negligible. This confirms Theorem 1 for the case of $M \geq 8$.

5.3 BER under fixed CSI uncertainty

Figure 7 depicts the BER comparison between the ML and the GD under fixed CSI uncertainty, with $(N, K, M) = (4, 2, 2)$, $L = 2, 4, 8, 12$ and $\epsilon^2 = 0.2$. Interestingly, it can be seen from this figure that at high SNRs, the GD outperforms the ML in terms of the BER. For example, as $L = 4$, the GD achieves the BER lower than the ML when $E_s/N_0 \geq 15$ dB. This is due to the fact that under the fixed CSI uncertainty, using the energy detection, the GD achieves better index detection performance than

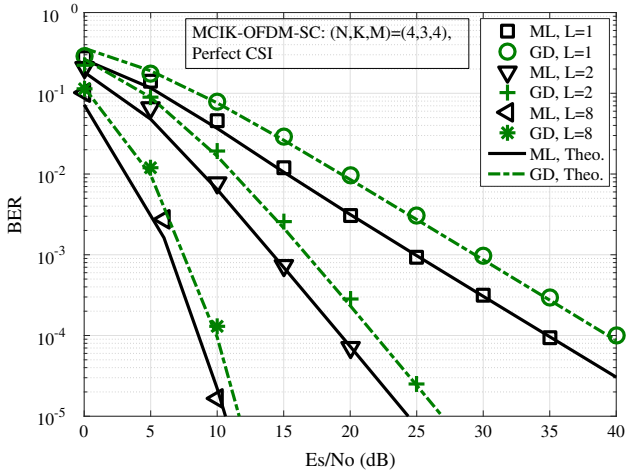

Fig. 5 BER comparison between the ML and the GD in MCIK-OFDM-SC under perfect CSI, with $(N, K, M) = (4, 3, 4)$ and $L = 1, 2, 8$

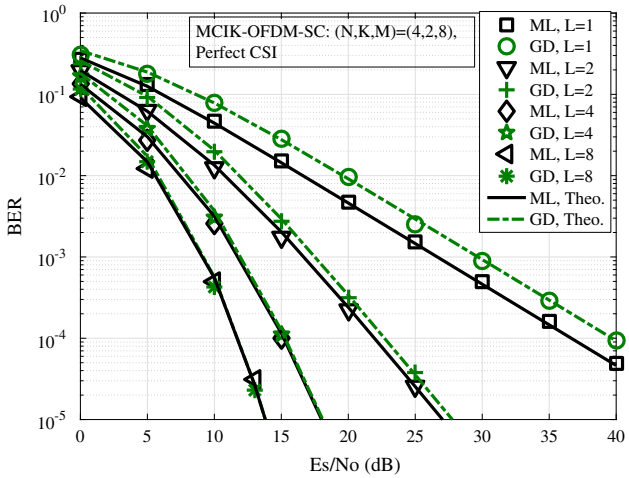

Fig. 6 BER comparison between the ML and the GD in MCIK-OFDM-SC under perfect CSI, with $(N, K, M) = (4, 2, 8)$ and $L = 1, 2, 4, 8$

its ML counterpart, leading to better BER performance, as theoretically proved in Sect. IV-B. Moreover, due to the fixed error variance, i.e., $\epsilon^2 = 0.2$, there exists error floors on the BERs of the two detectors. These floors get lower as L increases. This observations validate Theorem 2.

5.4 BER under MMSE variable CSI uncertainty

Figure 8 depicts the BER comparison between the GD and ML detectors under MMSE-based variable CSI uncertainty, with $(N, K, M) = (2, 1, 2)$ and $L = 1, 2, 4, 8$. As seen via Fig. 8, when L gets larger, the BERs of the two detectors become closer. However, the ML always outperforms the GD. In addition, the performance gap between them under variable CSI uncertainty gets smaller

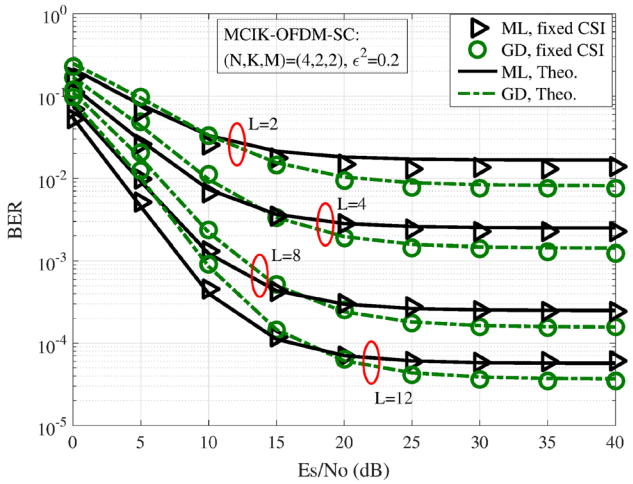

Fig. 7 BER comparison between the ML and the GD in MCIK-OFDM-SC under fixed CSI, with $(N, K, M) = (4, 2, 2)$, $L = 2, 4, 8, 12$ and $\epsilon^2 = 0.2$

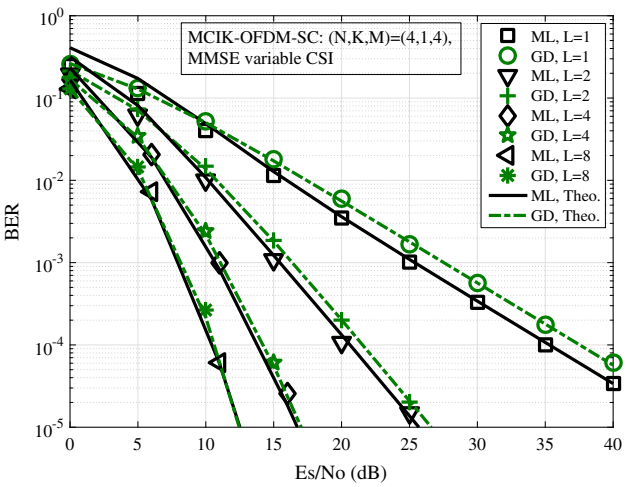

Fig. 9 BER comparison between the ML and the GD in MCIK-OFDM-SC under MMSE variable CSI uncertainty, with $(N, K, M) = (4, 1, 4)$ and $L = 1, 2, 4, 8$

than that under perfect CSI in Fig. 4. These observations validate Theorem 3 for $M = 2$.

Figure 9 compares the BER between the two detectors under MMSE variable CSI, when $(N, K, M) = (4, 1, 4)$ and $L = 1, 2, 4, 8$. Unlike the perfect CSI case, the BERs of the ML and the GD under this CSI condition quickly converge to each other as L increases even when $M = 4$. Similar to Fig. 6, as $L \geq 2$ there is a marginal gap in the BER between the two detectors. Hence, Theorem 3 with $M \geq 4$ is clearly validated.

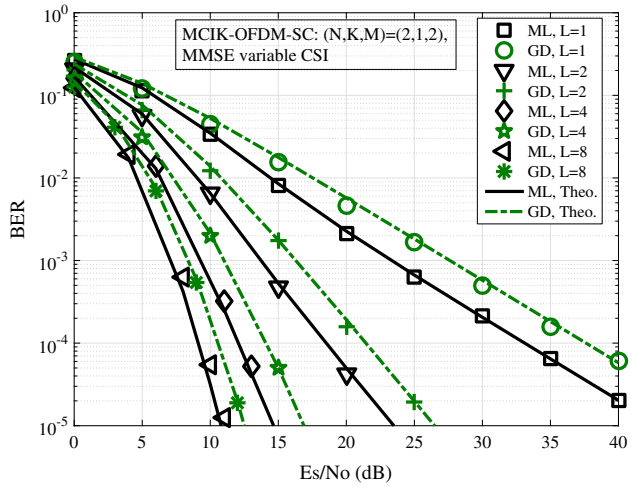

Fig. 8 BER comparison between the ML and the GD in MCIK-OFDM-SC under MMSE variable CSI uncertainty, with $(N, K, M) = (2, 1, 2)$ and $L = 1, 2, 4, 8$

6 Conclusions

We proposed a generalized framework for the BER analysis of MCIK-OFDM using either the GD or ML detector. Based on this, we derived tight, closed-form expressions for the BERs of MCIK-OFDM with the selection combining ML (or GD) receiver, taking effects of CSI uncertainty into account. We provided the asymptotic analysis to investigate impacts of imperfect CSI on their BERs. Furthermore, the BER comparison between the GD and ML detectors under various CSI conditions was presented, which allows to provide a theoretical guideline on the signal detection of MCIK-OFDM-SC under each specific CSI condition. For example, under MMSE-based variable CSI, the SC-based GD was shown to approach the SC-based ML in terms of the BER as the number of antennas increases and $M \geq 4$. More interestingly, under fixed CSI uncertainty and at high SNRs, the SC-based GD always outperforms the SC-based ML in terms of the BER for any value of M. Finally, the derived BER expressions and theoretical guideline are validated via simulation results. It is noteworthy that the derived expressions and proposed guideline for using the GD would be useful for various designs of the practical implementation of MCIK-OFDM. In our future work, we plan to investigate the performance of MCIK-OFDM-SC in combination with a number of diversity enhancement techniques, such as coordinate interleaving [8], repetition codes [11], and spreading matrix [14].

Appendix A

Proof of Lemma 1

The instantaneous SEP of the classical PSK symbol detection per sub-carrier α (denoted by $P_M(\alpha)$) is given by [26]

$$P_M(\alpha) \approx \frac{\xi}{12}\left[e^{-\frac{\rho\bar{\gamma}\hat{v}_\alpha}{1+\epsilon^2\bar{\gamma}}} + 3e^{-\frac{4\rho\bar{\gamma}\hat{v}_\alpha}{3\left(1+\epsilon^2\bar{\gamma}\right)}}\right], \tag{31}$$

where $\xi = 1$ for $M = 2$ and $\xi = 2$ for $M > 2$, and $\hat{v}_\alpha = \left|\hat{h}(\alpha)\right|^2$ which is chi-square distributed with degrees of freedom of two, .i.e, $\hat{v}_\alpha \sim \mathcal{X}_2^2$. Note that $\left|\hat{h}(\alpha)\right|^2 = \max_l \left|\hat{h}_l(\alpha)\right|^2$ and using the order statistics theory, the probability density function (PDF) of $\hat{v}_\alpha$ is given as

$$f_{\hat{v}}(x) = \frac{L}{a}e^{-\frac{x}{a}}\left(1 - e^{-\frac{x}{a}}\right)^{L-1}, \tag{32}$$

where $a = 1 - \epsilon^2$. Using (32), the MGF of $\hat{v}_\alpha$ can be obtained, after simple manipulations, as

$$\mathcal{M}_{\hat{v}}(t) = \frac{L!}{\prod_{l=1}^{L}(l - at)}. \tag{33}$$

Finally, applying the MGF approach to (31) and using (33), the average SEP of (31) is attained as (9).

Appendix B

Proof of Lemma 2

Let $b = \left|\hat{h}(\alpha)\right|$ and $Z = \left|\left|\hat{h}(\alpha)\right| + \tilde{e}(\alpha)\right|^2$. Assume that $\tilde{e}(\alpha) = c + jd$, where $c, d \sim \mathcal{N}(0, \epsilon^2/2)$, we obtain

$$Z = (b + c)^2 + d^2. \tag{34}$$

Let $Z' = 2Z/\epsilon^2 = \left[\sqrt{2}(b + c)/\epsilon\right]^2 + \left(\sqrt{2}d/\epsilon\right)^2$. Due to $\sqrt{2}(b + c)/\epsilon \sim \mathcal{N}\left(\sqrt{2}b/\epsilon, 1\right)$ and $\sqrt{2}d/\epsilon \sim \mathcal{N}(0, 1)$, Z' is distributed according to the noncentral chi-squared distribution with two degrees of freedom, i.e., $\mathcal{X}_2^2(\lambda)$, where $\lambda = 2b^2/\epsilon^2$ is the non-centrality parameter [31]. Thus, the MGF of Z' is given by [31]

$$\mathcal{M}_{Z'}(t) = \frac{e^{\frac{2b^2t/\epsilon^2}{1-2t}}}{1 - 2t}. \tag{35}$$

Finally, the MGF of Z can be computed, using $\mathcal{M}_{Z'}(t)$ in (35) as $\mathcal{M}_Z(t) = \mathcal{M}_{Z'}(\epsilon^2 t/2)$, which leads to (16).

References

1. Abu-alhiga, R., & Haas, H. (2009). Subcarrier-index modulation OFDM. In *Proceedings of IEEE Personal, Indoor and Mobile Radio Communications*, pp. 177–181.
2. Tsonev, D., Sinanovic, S., & Haas, H. (2011). Enhanced subcarrier index modulation (sim) ofdm. In *IEEE GLOBECOM Workshops (GC Wkshps),2011*, 728–732.
3. Basar, E., Aygolu, U., Panayirci, E., & Poor, H. V. (2013). Orthogonal frequency division multiplexing with index modulation. *IEEE Transactions on Signal Processing, 61*(22), 5536–5549.
4. Basar, E., Wen, M., Mesleh, R., Renzo, M. D., Xiao, Y., & Haas, H. (2017). Index modulation techniques for next-generation wireless networks. *IEEE Access, 5,* 16 693-16 746.
5. Ko, Y. (2014). A tight upper bound on bit error rate of joint OFDM and multi-carrier index keying. *IEEE Communications Letters, 18*(10), 1763–1766.
6. Basar, E. (2016). On multiple-input multiple-output OFDM with index modulation for next generation wireless networks. *IEEE Transactions on Signal Processing, 64*(15), 3868–3878.
7. Fan, R., Yu, Y. J., & Guan, Y. L. (2015). Generalization of orthogonal frequency division multiplexing with index modulation. *IEEE Transactions on Wireless Communications, 14*(10), 5350–5359.
8. Basar, E. (2015). OFDM with index modulation using coordinate interleaving. *IEEE Wireless Communications Letters, 4*(4), 381–384.
9. Kaddoum, G., Ahmed, M. F. A., & Nijsure, Y. (2015). Code index modulation: A high data rate and energy efficient communication system. *IEEE Communications Letters, 19*(2), 175–178.
10. Kaddoum, G., Nijsure, Y., & Tran, H. (2016). Generalized code index modulation technique for high-data-rate communication systems. *IEEE Transactions on Vehicular Technology, 65*(9), 7000–7009.
11. Luong, T. V., Ko, Y., & Choi, J. (2018). Repeated MCIK-OFDM with enhanced transmit diversity under CSI uncertainty. *IEEE Transactions on Wireless Communications, 17*(6), 4079–4088.
12. Choi, J. (2017). Coded OFDM-IM with transmit diversity. *IEEE Transactions on Communications, 65*(7), 3164–3171.
13. Le, T. T. H., Tran, X. N., Ngo, V.-D., & Le, M.-T. (2021). Repeated index modulation-OFDM with coordinate interleaving: Performance optimization and low-complexity detectors. *IEEE Systems Journal, 15*(3), 3673–3681.
14. Luong, T. V., & Ko, Y. (2018). Spread OFDM-IM with precoding matrix and low-complexity detection designs. *IEEE Transactions on Vehicular Technology, 67*(12), 11 619-11 626.
15. Zheng, B., Chen, F., Wen, M., Ji, F., Yu, H., & Liu, Y. (2015). Low-complexity ML detector and performance analysis for OFDM with in-phase/quadrature index modulation. *IEEE Communications Letters, 19*(11), 1893–1896.
16. Mao, T., Wang, Z., Wang, Q., Chen, S., & Hanzo, L. (2017). Dual-mode index modulation aided OFDM. *IEEE Access, 5,* 50–60.
17. Wen, M., Basar, E., Li, Q., Zheng, B., & Zhang, M. (2017). Multiple-mode orthogonal frequency division multiplexing with index modulation. *IEEE Transactions on Communications, 65*(9), 3892–3906.
18. Luong, T. V., Ko, Y., Vien, N. A., Nguyen, D. H. N., & Matthaiou, M. (2019). Deep learning-based detector for OFDM-IM. *IEEE Wireless Communications Letters, 8*(4), 1159–1162.
19. Wang, T., Yang, F., Song, J., & Han, Z. (2020). Deep convolutional neural network-based detector for index modulation. *IEEE Wireless Communications Letters, 9*(10), 1705–1709.

20. Van Luong, T., Ko, Y., Vien, N. A., Matthaiou, M., & Ngo, H. Q. (2020). Deep energy autoencoder for noncoherent multicarrier MU-SIMO systems. *IEEE Transactions on Wireless Communications, 19*(6), 3952–3962.
21. Luong, T. V., Ko, Y., Matthaiou, M., Vien, N. A., Le, M.-T., & Ngo, V.-D. (2021). Deep learning-aided multicarrier systems. *IEEE Transactions on Wireless Communications, 20*(3), 2109–2119.
22. Xu, C., Van Luong, T., Xiang, L., Sugiura, S., Maunder, R. G., Yang, L.-L., & Hanzo, L. (2022). Turbo detection aided autoencoder for multi-carrier wireless systems: Integrating deep learning into channel coded systems. *IEEE Transactions on Cognitive Communications and Networking, 8*(2), 600–614.
23. Van Luong, T., Zhang, X., Xiang, L., Hoang, T. M., Xu, C., Petropoulos, P., & Hanzo, L. (2022). Deep learning-aided optical IM/DD OFDM approaches the throughput of RF-OFDM. *IEEE Journal on Selected Areas in Communications, 40*(1), 212–226.
24. Khalid, A., Rashid, F., Tahir, U., Asif, H. M., & Al-Turjman, F. (2021). Multi-carrier visible light communication system using enhanced sub-carrier index modulation and discrete wavelet transform. *Wireless Personal Communications*. https://doi.org/10.1007/s11277-021-08121-y
25. Luong, T. V., & Ko, Y. (2018). Impact of CSI uncertainty on MCIK-OFDM: Tight, closed-form symbol error probability analysis. *IEEE Transactions on Vehicular Technology, 67*(2), 1272–1279.
26. Van Luong, T., & Ko, Y. (2017). A tight bound on BER of MCIK-OFDM with greedy detection and imperfect CSI. *IEEE Communications Letters, 21*(12), 2594–2597.
27. Crawford, J., Chatziantoniou, E., & Ko, Y. (2017). On the SEP analysis of OFDM index modulation with hybrid low complexity greedy detection and diversity reception. *IEEE Transactions on Vehicular Technology, 66*(9), 8103–8118.
28. Crawford, J., & Ko, Y. (2015). "Low complexity greedy detection method with generalized multicarrier index keying OFDM. In *IEEE Proceedings on Personal, Indoor and Mobile Radio Communications*, pp. 688–693.
29. Luong, T. V., & Ko, Y. (2017). Symbol error outage performance analysis of MCIK-OFDM over complex TWDP fading. In *Proc. Eur. Wireless*, pp. 1–5.
30. Chatziantoniou, E., Crawford, J., & Ko, Y. (2016). Performance analysis of a low-complexity detector for MCIK-OFDM over TWDP fading. *IEEE Communications Letters, 20*(6), 1251–1254.
31. Johnson, N., Kotz, S., & Balakrishnan, N. (1995). *Continuous univariate distributions* (Vol. 2). Wiley.

Vu-Duc Ngo received the Ph.D. degree from the Korea Advanced Institute of Science and Technology in 2011. From 2007 to 2009, he was a Co-Founder and the CTO of Wichip Technologies Inc., USA. Since 2009, he has been a Co-Founder and the Director of uVision Jsc, Vietnam. Since 2012, he has been serving as a BoM Member of the National Program on Research, Training, and Construction, High-Tech Engineering Infrastructure of Vietnam. He is currently a Lecturer with the School of Electrical and Electronics Engineering, Hanoi University of Science and Technology, and a Researcher with the MobiFone Research and Development Center, MobiFone Corporation, Vietnam. His research interests are in the fields of SoC, NoC design and verification, VLSI design for multimedia codecs, and wireless communications PHY layer. He was a recipient of the IEEE 2006 ICCES and the IEEE 2012 ATC Best Paper Award.

Thien Van Luong is currently a Lecturer with the Faculty of Computer Science, and a Leader of AIoT Lab (https://aiot.phenikaa-uni.edu.vn/), Phenikaa University, Vietnam. He was a Research Fellow with University of Southampton, U.K. Prior to that he obtained the Ph.D. degree at Queen's University Belfast, U.K., and the B.S. degree at Hanoi University of Science and Technology, Vietnam. His research interests include applied machine learning in signal processing and wireless communications.

Nguyen Cong Luong received the M.S. degree in electronic and telecommunication engineering from the Hanoi University of Science and Technology (HUST). His research interest includes the next generation networks.

Minh-Tuan Le was born in Thanh Hoa, Vietnam, in 1976. He received his B.E. degree in electronic engineering from Hanoi University of Science and Technology, Vietnam in 1999, M.S. degree and Ph.D. degree both in electrical engineering from Information and Communication University, which is currently the Department of Electrical and Engineering of Korean Advanced Institute of Science and Technology (KAIST), Daejon, Korea, in 2003 and 2007, respectively. From 1999 to 2001 and from 2007 to 2008 he worked as a lecturer at Posts and Telecommunication Institute of Technology (PTIT), Vietnam. From November 2012 to 2015, he worked at Hanoi Department of Science and Technology, Vietnam. He is currently working at MobiFone Reasearch and Development Center, MobiFone Corporation, Vietnam. His research interests include space-time coding, space-time processing, and MIMO systems. Dr. Le is the recipient of the 2012 ATC Best Paper Award from the Radio Electronics Association of Vietnam (REV) and the IEEE Communications Society. He is a member of IEEE.

Thi Thanh Huyen Le was born in Hanoi, Vietnam, in 1986. She received the B.Eng. and M.Sc. degrees in electronic engineering, and the Ph.D. degree from Le Quy Don Technical University, Hanoi, Vietnam, in 2010, 2014, and 2020, respectively. Since 2010, she has been a Lecturer with the Le Quy Don Technical University. Her research interests include MIMO, UAV, cooperative communications, and index modulation.

Xuan Nam Tran is currently a professor and head of the strong research group in advanced wireless communications in Le Quy Don Technical University Vietnam. He received his Master of Engineering (ME) in Telecommunications Engineering from University of Technology Sydney, Australia in 1998, and Doctor of Engineering in Electronic Engineering from The University of Electro-Communications, Japan in 2003. From November 2003 to March 2006 he was a research associate at the Information and Communication Systems Group, Department of Information and Communication Engineering, The University of Electro-Communications, Tokyo, Japan. Dr. Tran's research interests are in the areas of advanced technologies for wireless communications such as array signal processing, space-time communications, spatial and index modulation, cooperative communications, in-band full duplex (IBFD), NOMA, UAV-assisted communications and machine learning-based communication. He is the authors of 5 textbooks and reference books. Dr. Tran is a recipient of the 2003 IEEE AP-S Japan Chapter Young Engineer Award, and a co-recipient of two best papers from The 2012 International Conference on Advanced Technologies for Communications and The 2014 National Conference on Electronics, Communications and Information Technology. He is the member of the State Council for Professorship in Electricity-Electronics-Automation and Vice Chair of the Council for Information and Computer Science of the National Foundation for Science and Technology Development (NAFOSTED). He is a member of IEEE, IEICE and the Radio-Electronics Association of Vietnam (REV).